intensities. We obtained the highest FL for Q-CdS adsorbed onto GaAs for each of the three relative sizes of quantum dots. We suspect that this latter observation may be due to radiative recombination between electrons confined to the quantum dots with holes captured at the shallow acceptor level of the GaAs-quantum dot interface. With an eye toward future HEM device applications, this higher FL emission would suggest further study of functionalized Q-CdS adsorbed onto GaAs.

4. CONCLUSIONS

We have examined the FL spectra of AOT (dioctyl sulfoccinate) capped cadmium sulfide quantum dots (Q-CdS) deposited upon gold (Au), insulator (mica), and semiconductor (GaAs) substrates for their potential use in hybrid optoelectronic devices. Relative dot sizes were synthesized to increase from 1 to 5 nm with a respective increase in heptane concentration from 40 to 80 μL. Excitation and emission spectra are presented for the 200–400 nm and 400–700 nm ranges, respectively. For the smallest (40 μL heptane) quantum dots, a clear red shift in FL emission peak wavelength is observed from the Au, to mica, to GaAs substrate-based samples. For the midrange (70 μL) and largest (80 μL) Q-CdS samples, the longest emission peak wavelengths are observed for the quantum dots physisorbed to Au substrates with a subsequent decrease and then increase in emission wavelengths for the mica and GaAs substrate-based samples, respectively. Of the three types of substrates used, Q-CdS deposited upon GaAs exhibited the highest FL emission intensity, which bodes well for the possible integration of HEMs into next-generation device technology.

ACKNOWLEDGMENTS

The authors gratefully acknowledge the support of Prof. Isiah M. Warner and his postdoctoral research assistant, Dr. Mark Lowry, of the LSU Department of Chemistry, for synthesis of the cadmium sulfide quantum dots and assistance with the fluorescence measurements. This work was partially supported by funding from the LSU Center for Computation & Technology and the Department of Energy (Award No. DE-FG02-97ER45648).

REFERENCES

1. Y. Yin and A.P. Alivisatos, Colloidal nanocrystal synthesis and the organic-inorganic interface, Nature 437 (2005), 664–670.
2. P.O. Anikeeva, J.E. Halpert, M.G. Bawendi, and V. Bulovic, Electroluminescence from a mixed red-green-blue colloidal quantum dot monolayer, Nano Lett 7 (2007), 2196–2200.
3. G. Konstantatos, L. Levina, A. Fischer, and E.H. Sargent, Engineering the temporal response of photoconductive photodetectors via selective introduction of surface trap states, Nano Lett 8 (2008), 1446–1450.
4. K. Sun, M. Vasudev, H.S. Jung, J.Y. Yang, A. Kar, Y. Li, K. Reinhardt, P. Snee, M.A. Stroscio, and M. Dutta, Applications of colloidal quantum dots, Microelectron J 40 (2009), 644–649.
5. A.N. Cao, Z. Liu, S.S. Chu, M.H. Wu, Z.M. Ye, Z.W. Cai, Y.L. Chang, S.F. Wang, Q.H. Gong, and Y.F. Liu, A facile one-step method to produce graphene-cds quantum dot nanocomposites as promising optoelectronic materials, Adv Mater 22 (2010), 103–106.
6. C.P. Han and H.B. Li, Host-molecule-coated quantum dots as fluorescent sensors, Anal Bioanal Chem 397 (2010), 1437–1444.
7. M.F. Hossain, S. Biswas, and T. Takahashi, Study of cds-sensitized solar cells, prepared by ammonia-free chemical bath technique, Thin Solid Films 518 (2009), 1599–1602.
8. P. Sudhagar, J.H. Jung, S. Park, R. Sathyamoorthy, H. Ahn, and Y.S. Kang, Self-assembled cds quantum dots-sensitized tio2 nanospheroidal solar cells: Structural and charge transport analysis, Electrochim Acta 55 (2009), 113–117.
9. M. Shalom, S. Ruhle, I. Hod, S. Yahav, and A. Zaban, Energy level alignment in cds quantum dot sensitized solar cells using molecular dipoles, J Am Chem Soc 131 (2009), 9876–9877.
10. G. Konstantatos and E.H. Sargent, Solution-processed quantum dot photodetectors, Proc IEEE 97 (2009), 1666–1683.
11. J. Barman and K.C. Sarma, Structural and optical properties of cds nanoparticles, Indian J Phys Proc Indian Assoc Culti Sci 82 (2008), 855–862.
12. S.R. Stebbing, R.W. Hughes, and R.A. Reynolds, Sizing, stoichiometry and optical absorbance variations of colloidal cadmium sulphide nanoparticles, Adv Colloid Interface Sci 147–148 (2009), 272–280.
13. H.L. Lee, A.M. Issam, M. Belmahi, M.B. Assouar, H. Rinnert, and M. Alnot, Synthesis and characterizations of bare cds nanocrystals using chemical precipitation method for photoluminescence application, J Nanomater (2009), 9.
14. R. Paul, P. Kumbhakar, and A.K. Mitra, Visible photoluminescence of mwcnt/cds nanohybrid structure synthesized by a simple chemical process, Mater Sci Eng B-Adv Funct Solid-State Mater 167 (2010), 97–101.
15. L.E. Shea-Rohwer, J.E. Martin, and D.F. Kelley, Increasing the luminescent quantum yield of cds nanoparticles having broadband emission, J Electrochem Soc 157 (2010), J1–J7.
16. S. Ogawa, F.R.F. Fan, and A.J. Bard, Scanning-tunneling-microscopy, tunneling spectroscopy, and photoelectrochemistry of a film of q-cds particles incorporated in a self-assembled monolayer on a gold surface, J Phys Chem 99 (1995), 11182–11189.
17. Y.F. Chen and Z. Rosenzweig, Luminescent cds quantum dots as selective ion probes, Anal Chem 74 (2002), 5132–5138.
18. T. Daniels-Race and S. Thiruvengadam, Characterization of aot capped cadmium sulfide quantum dots using fluorescence spectroscopy, Microwave Opt Technol Lett 52 (2010), 912–913.
19. Jobin Yvon Horiba Inc., Available at: http://www.Jobinyvon.Com/usadivisions/fluorescence/product/flogcat.Pdf, Images obtained from 2007 product catalog.
20. M.A. Reed and T. Lee (Eds.), Molecular nanoelectronics, American Scientific Publishers, 2003.

A SIMPLE FBG SENSOR FOR STRAIN–TEMPERATURE DISCRIMINATION

Parne Saidi Reddy,[1] R. L. N. Sai Prasad,[1] D. Sen Gupta,[1] M. Sai Shankar,[1] K. Srimannarayana,[1] Umesh Tiwari,[2] and Vandana Mishra[2]

[1] Department of Physics, National Institute of Technology Warangal, Warangal 506004, Andhra Pradesh, India; Corresponding author: sadashivareddy1@gmail.com

[2] Photonics, Central Scientific Instruments Organisation, Chandigarh, India

Received 9 August 2010

ABSTRACT: *A simple sensor using half the length of a 3-cm fiber Bragg grating embedded on a cantilever is proposed for the simultaneous measurement and discrimination of strain and temperature. The response of the sensor is linear from 30 to 200°C, and its strain and temperature sensitivities are found to be 3.38 pm/μm 19.05 pm/°C, respectively.* © 2011 Wiley Periodicals, Inc. Microwave Opt Technol Lett 53:1021–1024, 2011; View this article online at wileyonlinelibrary.com. DOI 10.1002/mop.25901

Key words: *fiber Bragg grating sensor; strain sensor; temperature sensor; strain and temperature discrimination; cantilever beam*

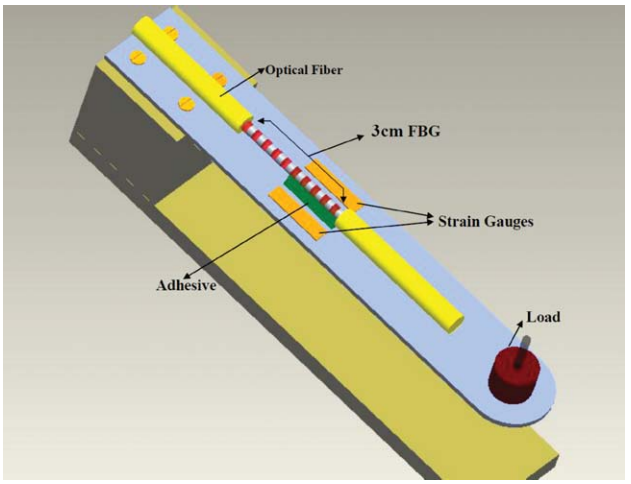

Figure 1 Schematic of proposed sensor head. [Color figure can be viewed in the online issue, which is available at wileyonlinelibrary.com]

1. INTRODUCTION

The fiber Bragg grating (FBG) sensors have proved to be very successful as substitutes for the traditional fiber-based sensors. Their small size and inconspicuous presence are very promising in applications that require the physical advantages of optical fibers such as EMI immunity, distributed sensing, light weight, radiation, and corrosion tolerance. In addition, FBGs have a unique optical advantage that offers immunity to intensity fluctuations, polarization changes, and connection losses. The sensing information through FBG is wavelength encoded.

The response of FBG is simultaneously sensitive to both strain and temperatures, and a number of techniques have been reported to measure and discriminate these parameters on a single measurement of Bragg wavelength shift. A number of schemes have been proposed to overcome this limitation. The schemes can be classified into two classes: (1) single FBG sensor schemes [1–3] and (2) combination schemes, which utilize two or more FBGs [4–6]. However, the use of more than one fiber grating element increases the system complexity, cost and complicates the fabrication of the sensor head.

This article proposes a new sensor head design making use of single FBG for simultaneous measurement and discrimination of strain and temperature.

2. SENSOR DESIGN AND FABRICATION

The schematic of the designed sensor head is shown in Figure 1. It consists of a cantilever with rectangular stainless steel plate of 25-cm length and 4-cm width with thickness of 3 mm. An FBG of length 3 cm, fabricated at CSIO, Chandigarh, India [7], with a center wavelength of 1555.6 nm is taken, and exactly half of it (FBG_1) is glued at the center of the steel plate parallel to the length from 1 to 2.5 cm from the fixed end using a permanent instant high-temperature adhesive, whereas the remaining half (FBG_2) is allowed free. The reflection spectrum of which is shown in Figure 2. Four strain gauges are pasted on the plate, two on both sides of the glued FBG portion and two exactly at the bottom of the plate, forming a bridge, for making strain measurements.

3. THE PRINCIPLE

When one half of a 3-cm FBG is glued to a metal plate and the other half left free, and the plate is subjected to load, the portion of the FBG that is attached gets strained and there will be a wavelength shift of $\Delta\lambda$, whereas the light reflected from the free portion does not suffer any shift. When the strain is increased, the shift also increases accordingly; thereby, the reflected spectrum from the sensor shows two peaks, one remains constant, whereas the other shifts according to the applied strain. The separation between them is proportional to the strain produced.

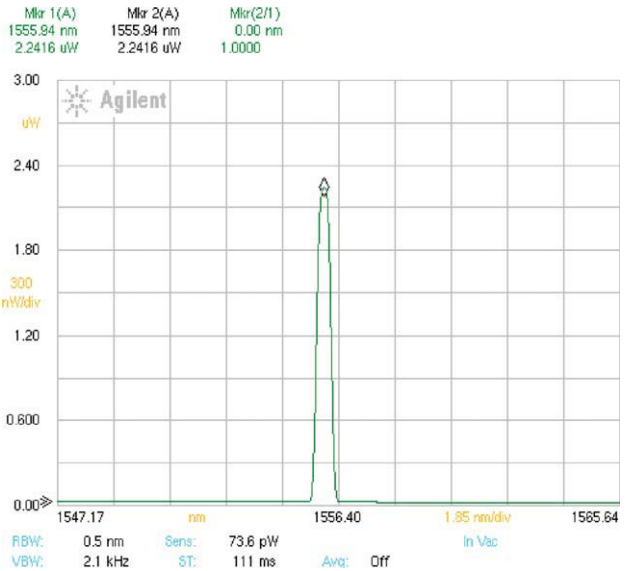

Figure 2 Reflected Bragg wavelength spectrum of FBG used in the sensor head. [Color figure can be viewed in the online issue, which is available at wileyonlinelibrary.com]

When such sensor is subjected to temperature at constant strain, the glued portion of the FBG responds to both temperature and strain, whereas the free portion responds only to temperature, and the shift in the wavelength in the reflected spectrum varies accordingly. Making these two observations, the strain and temperature can be discriminated.

The bending of cantilever loaded at the endpoint develops mechanical strain given by:

$$\varepsilon_i = \frac{2\Delta l_i}{l}, \tag{1}$$

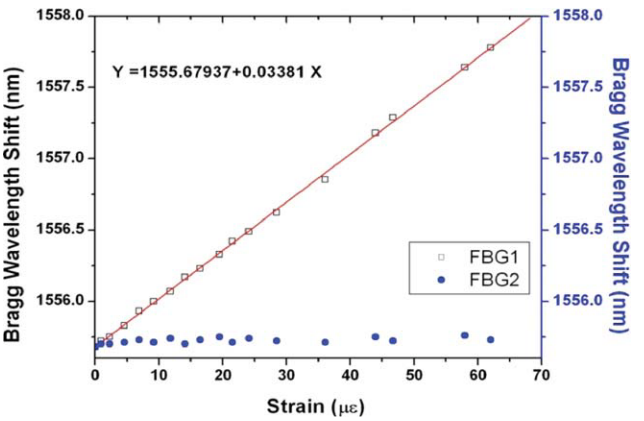

Figure 3 Wavelength response of the sensor to applied strain (at constant temperature 30°C). [Color figure can be viewed in the online issue, which is available at wileyonlinelibrary.com]

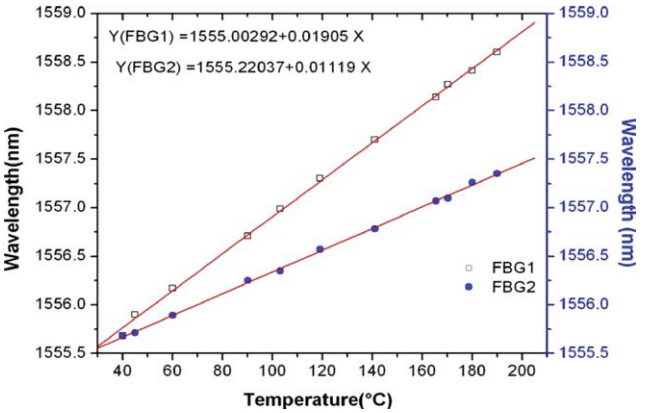

Figure 4 Wavelength response of the sensor to applied temperature (at constant strain of 10 $\mu\varepsilon$). [Color figure can be viewed in the online issue, which is available at wileyonlinelibrary.com]

where Δl_i is the elongation of the ith grating half and l is the length of the whole grating.

The average strain of the FBG is given by:

$$\varepsilon = \frac{\Delta l_1 + \Delta l_2}{l}, \tag{2}$$

where Δl_1 is the elongation of the FBG1 and Δl_2 is the elongation of the FBG2.

The Bragg wavelength shift of each grating half in terms of the average strain and temperature changes can be expressed as [8]:

$$\Delta\lambda_1 = K_{\varepsilon 1}\varepsilon + K_{T1}\Delta T \quad \text{and} \quad \Delta\lambda_2 = K_{\varepsilon 2}\varepsilon + K_{T2}\Delta T. \tag{3}$$

From these equations, it can be seen that the two gratings halves respond differently to the applied strain and temperature changes, so that the Bragg reflection from the grating peak will split into two.

4. RESULTS AND DISCUSSION

The response of the sensor was measured by subjecting it independently to strain and temperature. Figure 3 shows the sensor response to wavelength. Figure 4 shows the results of the experiment in which the temperature was kept constant at 30°C, whereas the strain applied to the sensor head is varied. It is seen that the Bragg reflected peak splits into two, and the wavelength separation between the peaks is increased with applied strain up to 62 $\mu\varepsilon$. The response of the FBG_1, which is glued to the cantilever, is linear with applied strain, whereas the strain response of the FBG_2 is found equal to zero. From these experimental data, strain coefficients of the FBG_1 and FBG_2 are calculated as $K\varepsilon_1 = 3.38$ pm/$\mu\varepsilon$ and $K\varepsilon_2 = 0$ pm/$\mu\varepsilon$, respectively.

Figure 4 shows the experimental results for the discrimination of the strain and temperature coefficients. In this, the applied strain is kept constant at 10 $\mu\varepsilon$, whereas the temperature was changed from 30 to 200°C. The slopes of the response curves of the FBG portions are different, indicating that FBG_1 is responding to both temperature and strain, whereas FBG_2 is responding only to temperature. The spectral response of the sensor indicating the split in the Bragg wavelength reflected peaks at various temperatures is shown in Figure 5. The temperature coefficients of FBG_1 and FBG_2 from the experimental data are found to be $K_{T1} = 19.05$ pm/°C and $K_{T2} = 11.19$ pm/°C, respectively.

The experimental observations on the responses of FBG_1 and FBG_2 of the sensor head to strain and temperature permit us to write a well-conditioned system of two equations for ΔT and $\Delta\varepsilon$ given in the form of matrix as [9].

$$\begin{bmatrix}\Delta T \\ \Delta\varepsilon\end{bmatrix} = \frac{1}{B}\begin{bmatrix}K\varepsilon_2 & -K\varepsilon_1 \\ K_{T2} & K_{T1}\end{bmatrix}\begin{bmatrix}\Delta\lambda_1 \\ \Delta\lambda_2\end{bmatrix}, \tag{4}$$

where $B = K\varepsilon_2 * K_{T1} - K\varepsilon_1 * K_{T2}$.

The matrix coefficients are found from the slopes of the experimental measured data shown in Figures 3 and 4 and take the form

$$\begin{bmatrix}\Delta T \\ \Delta\varepsilon\end{bmatrix} = -\frac{1}{36.48}\begin{bmatrix}0 & -3.38 \\ -11.19 & 19.05\end{bmatrix}\begin{bmatrix}\Delta\lambda_1 \\ \Delta\lambda_2\end{bmatrix}. \tag{5}$$

These preliminary results have demonstrated that the proposed sensor head could perform well for the simultaneous measurement and discrimination of strain and temperatures.

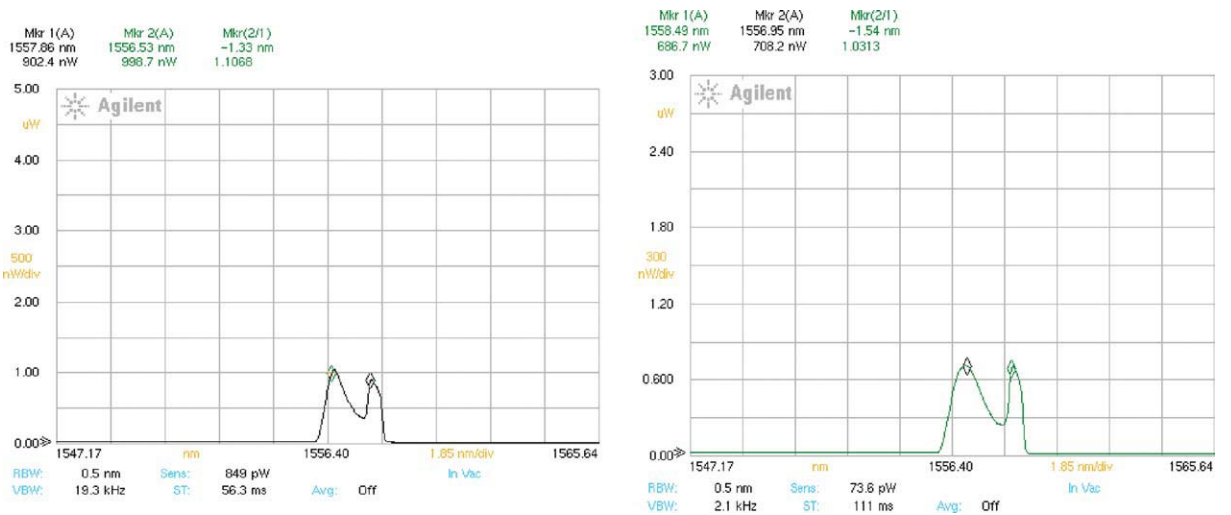

Figure 5 Spectral response of the Bragg reflected peak at different temperatures: (a) 145°C and (b) 185°C. [Color figure can be viewed in the online issue, which is available at wileyonlinelibrary.com]

5. CONCLUSION

A FBG sensor head capable of simultaneous measurement and discrimination of strain and temperature is demonstrated making use of single FBG. The experimental observations reveal that the response of the sensor is found to be linear over wide ranges of applied temperature and strain. The temperature and strain sensitivities of the sensor are found to be 19.05 pm/°C and 3.38 pm/μs, respectively.

ACKNOWLEDGMENTS

The authors thank Dr. Nehar Singh Mehla and CSIO Chandigarh, India, for providing the fiber Bragg gratings.

REFERENCES

1. W. Zhou, C.-L. Zhao, X. Dong, S. Zhang, C.C. Chan, and P. Shun, Simultaneous measurement of force and temperature based on a half corroded FBG, Microwave Opt Technol Lett 52 (2010), 2020–2023.
2. R. Aashia, K.V. Madav, B. Srinivasan, and S. Asokan, Strain-temperature discrimination using a single fiber Bragg grating, IEEE Photon Technol Lett 22 (2010), 778–780.
3. B.-O. Guan, H.-Y. Tam, H.L.W. Chan, C.-L. Choy, and M.S. Demokan, Discrimination between strain and temperature with a single fiber Bragg grating, Microwave Opt Technol Lett 33 (2002), 200–203.
4. Y. Zhao and Y. Liao, Discrimination methods and demodulation techniques for fiber Bragg grating sensor, Opt Lasers Eng 41 (2004), 1–18.
5. S.O. Park, B.W. Jang, Y.G. Lee, C.G. Kim, and C.Y. Park, Simultaneous measurement of strain and temperature using a reverse index fiber Bragg grating sensor, Meas Sci Technol 21 (2009), 1–7.
6. O. Frazao, R. Oliveira, and I. Dias, A simple smart composite using fiber Bragg grating sensors for strain and temperature discrimination, Microwave Opt Technol Lett 51 (2009), 35–238.
7. S.K. Mondal, V. Mishra, U. Tiwari, G.C. Poddar, N. Singh, S.C. Jain, S.N. Sarkar, and P. Kapur, Embedded dual fiber Bragg grating sensor for simultaneous measurement of temperature and load with enhanced sensitivity, Microwave Opt Technol Lett 51 (2009), 1621–1624.
8. H. Xu, X. Dong, Z. Yang, K. Ni, P. Shum, C. Lu, and H.Y. Tam, Simple FBG sensor head design for strain-temperature discrimination, Optoelectronics and Communication Conference (OECC), 978-1-4244-4 103/07/09; 2009.
9. A. Rahaman and S. Asokan, Fiber Bragg grating sensors: New ideas on strain and temperature discrimination, Int J Smart Sens Intell Syst 3 (2010), 109–117.

A NEW DIFFERENTIAL STACKED SPIRAL INDUCTOR WITH IMPROVED SELF-RESONANCE FREQUENCY

Joonchul Kim, Byungjae Nam, and Hyeongdong Kim
Department of Electronics and Computer Engineering, Hanyang University, 17, Haengdang-dong, Sungdong-gu, Seoul 133-791, Korea; Corresponding author: hdkim@hanyang.ac.kr

Received 9 August 2010

ABSTRACT: *A new silicon-based differential stacked spiral inductor (DSSI) was implemented using a standard 0.18-μm complimentary metal-oxide semiconductor technology. Based on the measured two-port S-parameter using a standard de-embedding procedure, the self-resonance frequency,* f_{sr}*, and quality factor,* Q*, of the new DSSI were compared with a conventional DSSI. The* f_{sr} *of the new DSSI was nearly twice as high as that of the conventional DSSI, and the* Q *value of the new DSSI was also enhanced.* © 2011 Wiley Periodicals, Inc. Microwave Opt Technol Lett 53:1024–1026, 2011; View this article online at wileyonlinelibrary.com. DOI 10.1002/mop.25900

Key words: *CMOS inductor; differential stacked spiral inductor; parasitic capacitance; self-resonance frequency*

1. INTRODUCTION

Miniaturization is a desirable aspect of monolithic circuit integration, particularly for radiofrequency (RF) integrated circuits

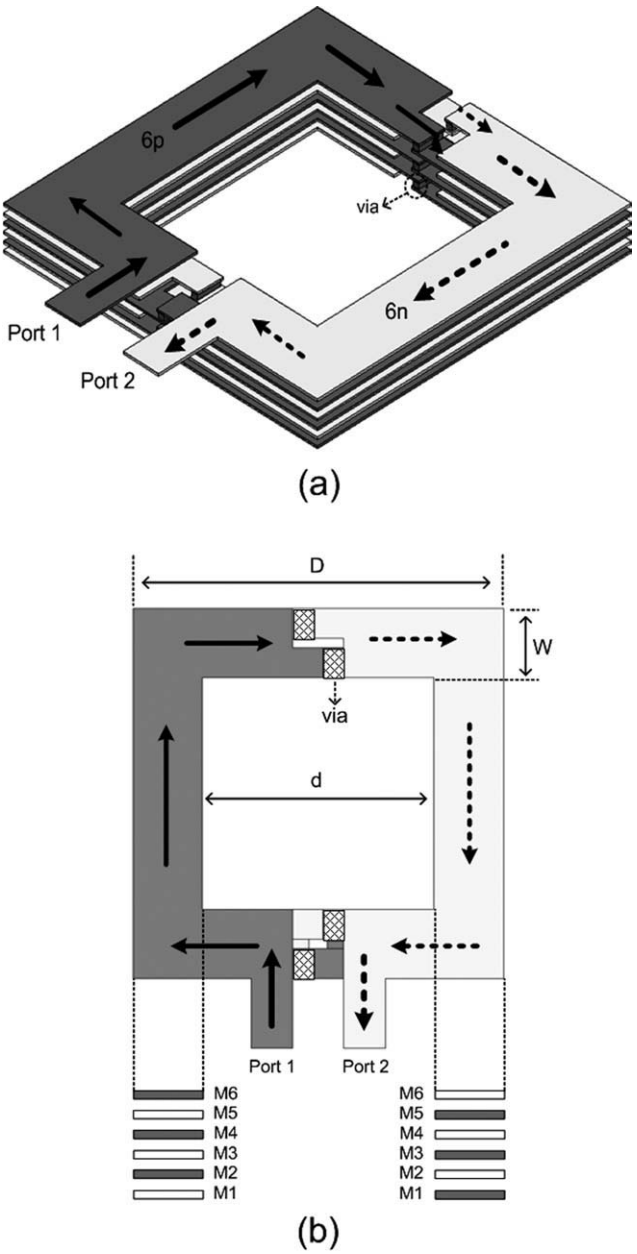

Figure 1 Configuration of the conventional DSSI: (a) Overall view and (b) top and side views